Enhanced spectral resolution via externally dispersed interferometry

Jerry Edelstein[a], David Erskine[b], Martin Sirk[a], Andrew Vanderburg[a], Edward H. Wishnow[a]
[a]Space Sciences Laboratory, University of California, Berkeley CA, USA 94720-7450
[b]Lawrence Livermore National Laboratory, Livermore CA, USA

ABSTRACT

Externally dispersed interferometry (EDI) uses a hybrid spectrometer that combines a Michelson interferometer in series with a grating spectrometer. EDI provides a means of deriving spectral information at a resolution substantially higher than that provided by the grating spectrograph alone. Near IR observations have been conducted using the Triplespec spectrometer mounted on the 5m Hale telescope. Spectra have been reconstructed at a resolution of ~27000 where the resolution of Triplespec is ~2700. Progress in the development of the EDI technique is reported herein emphasizing studies related to the accuracy of the reconstructed spectra.

Keywords: High resolution spectroscopy, externally dispersed interferometry, Doppler velocimetry

1. INTRODUCTION

Externally Dispersed Interferometry (EDI) is a technique that permits recovery of spectral features otherwise unobserved due to the resolution limits of grating spectrographs.[1--4] EDI also has been proposed and demonstrated as a method for measuring stellar radial velocities with high accuracy.[5--9] EDI combines a Michelson interferometer in series with a grating spectrometer. Glass etalons provide the optical path difference in one arm of the interferometer and a sinusoidal transmission pattern as a function of frequency (wavenumber) is imposed on the stellar spectrum. The interferometer is stepped over a series of sub-wavelength "phase" steps, creating a Moiré pattern between the interferometer and the stellar spectrum. By finding the amplitude and phase of this pattern at every frequency element of the spectrometer, the stellar spectrum can be reconstructed at a resolution much higher than that of the "native" dispersing spectrograph. Figure 1 shows a schematic diagram of an EDI instrument.

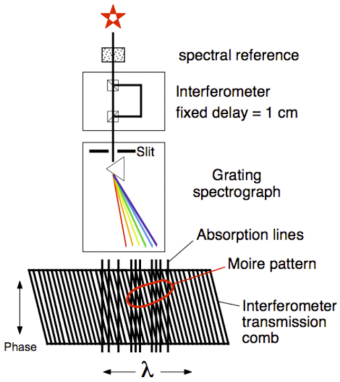

Figure 1 Schematic diagram of an EDI. The sinusoidal transmission comb of the interferometer is imposed on the stellar spectrum yielding a Moiré pattern. As the optical path is varied the Moiré pattern shifts and spectral information at high resolution can be deduced.

The instrument lineshape function of a grating spectrograph is determined by the slit width and the focusing properties of the optical system. The Fourier transform of the lineshape function is the modulation transfer function which has units of intensity as a function of optical delay (cm) or equivalently, spectral features per wavenumber (cm^{-1}). EDI uses a set of optical delays, and the measured Moiré patterns, to construct a high resolution spectrum. This paper describes work-in- progress on understanding the accuracy of the reconstructed spectrum.

2. NEAR IR SPECTRA FROM MT. PALOMAR

A series of EDI measurements was made using TEDI (TripleSpec Exoplanet Discovery Instrument), an infrared interferometer, in series with Triplespec, a near-IR echelle spectrometer for the Hale telescope.[9] A measurement set consisted of recording fringes using eight glass etalons with different thicknesses. Measurements on each etalon involved ten phase steps of the optical path difference, where each phase step had a 5 sec exposure time. Figure 2 shows one full order of the echelle spectrum. For these observations light from a Th-Ar lamp was combined with the starlight (kap CrB) for calibration purposes. The EDI technique yielded a resolution of $\lambda/\Delta\lambda$ ~27000 from a resolution ~2700 spectrometer. In the examples discussed here, the stellar source is used to obtain the atmospheric transmission spectrum. A model of atmospheric transmission at a resolution comparable to the EDI spectrum is also shown for comparison.[10]

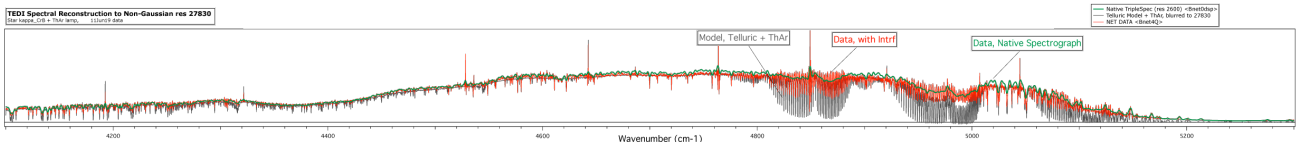

Figure 2. EDI spectrum from TripleSpec. Data extends from L-to-R from 2.44 to 1.89 μm. The green curve shows the R~2700 TripleSpec spectrum, the red curve shows the EDI reconstructed spectrum at R~27000, and the black curve shows a model telluric spectrum.

In order to compare the accuracy of the reconstructed spectrum, an EDI spectrum and a model spectrum were both fitted with a set of Gaussian lines with a fixed width (σ=0.21 cm^{-1}). Portions of these spectra (stellar source V* gam UMi) in the region of the atmospheric CO_2 band are shown in Figure 3. The line center frequencies of the reconstructed spectra are plotted against those of the model in the left panel of Figure 4. The fitted line centers correspond quite well to those of the model with an error in fitting the line frequency of 0.025 cm^{-1}, and $\lambda/\Delta\lambda$ is ~190000. The right panel shows a comparison of fitted line strengths. The fractional error in fitting the line strengths is 0.12.

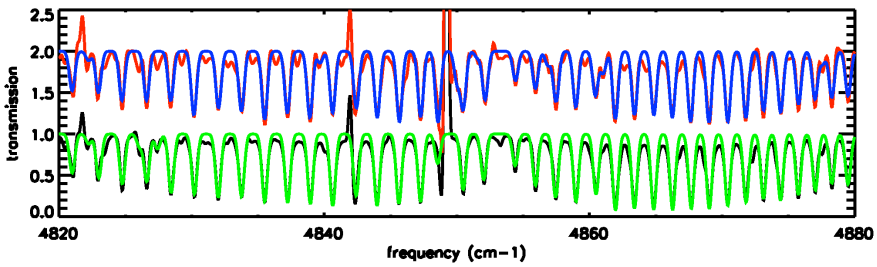

Figure 3. Reconstructed and model spectra. The upper red curve is the EDI spectrum (using seven etalons, spectral resolution ~19000) and the blue curve is the set of fitted Gaussians. The lower black curve is the model spectrum and the green curve is the set of fitted Gaussians. The emission features are Th-Ar calibration lines.

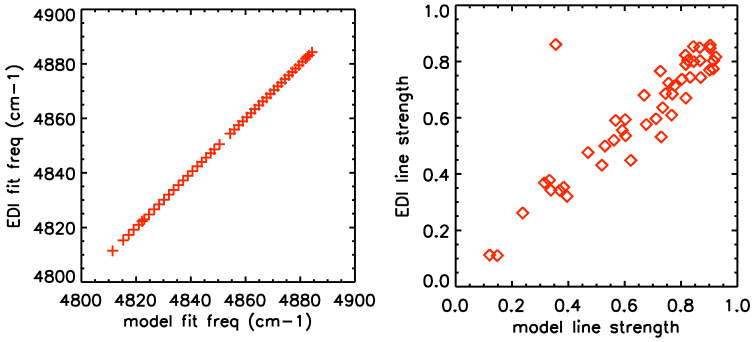

Figure 4. Comparisons of Gaussian lines fitted to EDI and model spectra. Left panel, fitted line centers; the error of the measurements compared to the model is 0.025 cm^{-1}. Right panel, fitted line strengths; the fractional error in fitting line strengths is 0.12. The errant point is from the large absorption feature near the Th-Ar emission line, it is excluded from the calculation of the error.

3. INTERFEROMETER DELAY DETERMINATION

To derive high resolution spectral information, it is essential to accurately determine the interferometer optical delay. In the TEDI system this is done by comparing theoretical fringes from atmospheric and Th-Ar spectral lines (artificially blurred to the "native" spectrometer resolution, but dispersionless) to measured fringes. Figure 5 shows such a comparison for delays produced by a glass etalon. A cubic fit to the delay vs. frequency graph gives an appropriate model for the dispersion of the 46 mm thick fused silica etalon. In the figure the stronger lines are represented by larger circles; generally these are due to Th-Ar emission lines. The phase difference vs. frequency curve is used to assemble reconstructed spectra across a wide simultaneous optical bandwidth.

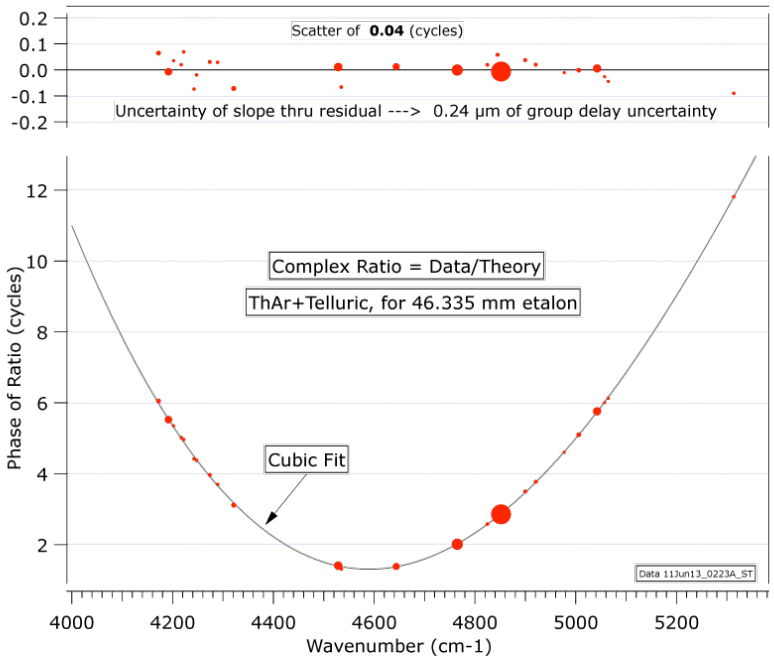

Figure 5. Phase difference between measurements and theory vs. frequency. The upper panel shows residuals.

The group delay describes the periodicity of the interferometer comb as a function of wavenumber. It is the absolute value of the derivative of the phase difference vs. frequency curve above. The group delay is also the quantity used in Doppler velocimetry applications of EDI. Figure 6 shows the group delay and the uncertainty in the group delay. The uncertainty of the group delay is estimated by the uncertainty of the slope of the best fit line through the phase residuals. The 0.24 µm uncertainty thus determined is much smaller than an integer fringe (1 wave or 2.2 µm).

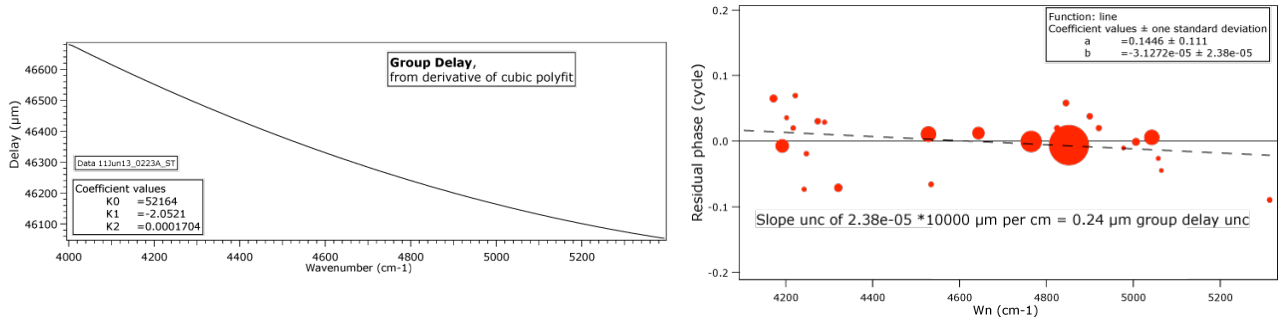

Figure 6. Left panel, group delay vs. frequency. Right panel, error in the linear fit to the residuals of the phase vs. frequency plot.

4. EFFECT OF DELAY ERRORS ON THE SPECTRAL LINESHAPE

Errors in the determination of the optical path delay lead to distortions in the reconstructed spectrum. A numerical examination of this issue is shown in Figure 7. The curves on the left show sinusoids associated with seven etalons. The sinusoids are multiplied by an envelope curve based on the "native" grating spectrometer lineshape. In the upper left panel the phases of the etalon curves are properly aligned and the synthesized lineshape that results from the addition of these waveforms, with Gaussian weighting (upper right panel) is sharp and symmetric. The lower left panel shows etalon waveforms that are deliberately misaligned. In this case, each etalon wave packet has a random shift selected from a normal distribution with a standard deviation equal to 10% of the FWHM of the "native" spectrograph resolution. The lower right panel shows the resulting distorted lineshape function.

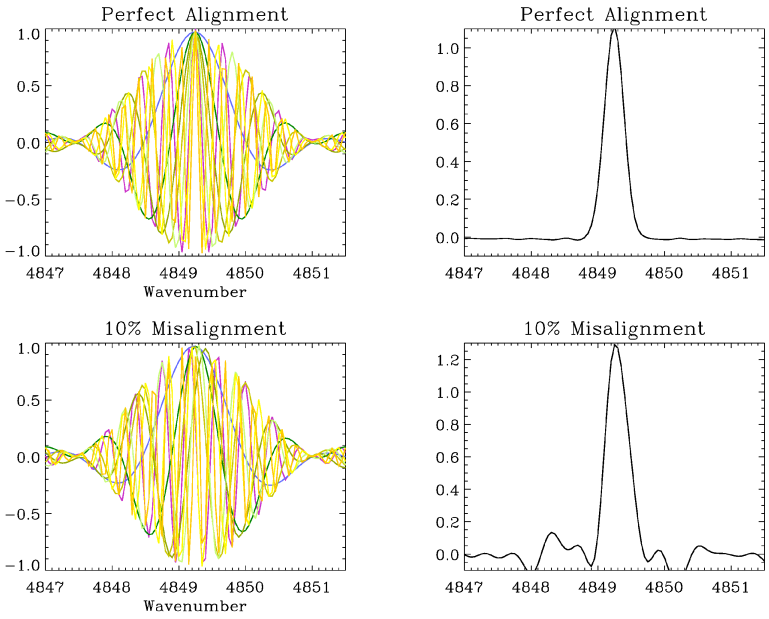

Figure 7. Simulation of distortions in the instrument lineshape due to wave packet alignment error. Upper left, etalon wave packets correctly aligned; upper right, the synthesized lineshape. Lower left, etalon wave packets with randomly distributed shifts; lower right, the resulting distorted synthesized lineshape.

A numerical study of how the synthesized lineshape is affected by waveform alignment error has been performed. A set of reconstructed lines using 1000 trials where the magnitude of the phase shifts are 0, 2.5, 5, and 10% of the "native" spectrograph resolution are shown by the solid curve. A set of 1000 trials for lines synthesized with phase shifts of 0, 2.5, 5, and 10% of a cycle of the etalon sinusoids are shown by dashed curves. In both cases, the set of sinusoids is combined with Gaussian weighting to obtain a Gaussian line, as in the upper right curve of Figure 7. The upper panel shows the standard deviation of sets of shifted line center frequencies as compared to the unshifted frequency. The middle panel shows the median values of sets of shifted linewidths divided by the width of the unshifted line. The lower panel shows the median values of the standard deviation of regions beyond +/- 3 linewidths compared to the unshifted line. The standard deviation is presented as a percentage of the line peak height. This quantity indicates the amount of ringing in the wings of the reconstructed line. Median values are used as the distributions tend to be asymmetrical. These studies show that distortions in the reconstructed spectrum are comparable to, or less than, the errors in the wave packet alignment..

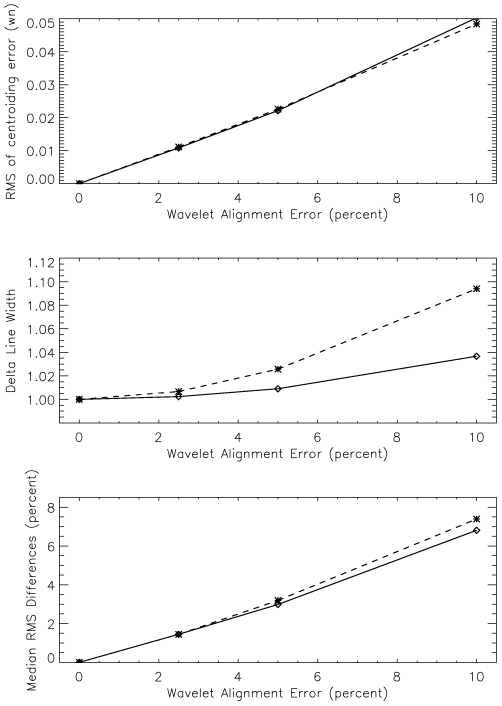

Figure 8. Results of numerical simulations of reconstructed lineshapes as a function of wave packet alignment error. Solid lines indicate random delay shifts with 0, 2.5,5, and 10% of the "native" spectrograph resolution; dashed lines indicate random delay shifts with 0, 2.5, 5, and 10% of a cycle of the etalon sinusoid. Upper panel, standard deviations of sets of shifted line center frequencies as compared to the unshifted line. Middle panel, standard deviations of sets of shifted line widths compared to the unshifted width. Bottom panel, standard deviations of regions beyond +/- 3 linewidths as compared to the unshifted line. The standard deviation is divided by the peak height.

5. A GAP IN THE MODULATION TRANSFER FUNCTION

The spectral information that becomes accessible using EDI is shown in the modulation transfer function (MTF) picture below. This curve is the Fourier transform of the lineshape and it has dimensions intensity vs. spectral features per wavenumber (or delay in cm, as in an FTS). Here the "native" spectrograph function is shown by the narrow Gaussian, the coverage of delays of the etalons are shown by the red curves (with the addition of an eighth etalon), and the dashed Gaussian is the desired MTF; it is obtained by weighting the contributions of the various etalons accordingly.

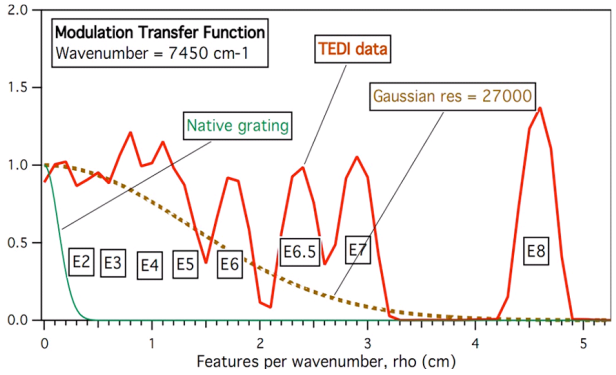

Figure 9. The modulation transfer function and the contributions of the etalons. The thin narrow curve near the origin, is the MTF of the "native" spectrograph, the red curve shows the contributions of the etalons, the dashed curve is the MTF of the reconstructed spectrum.

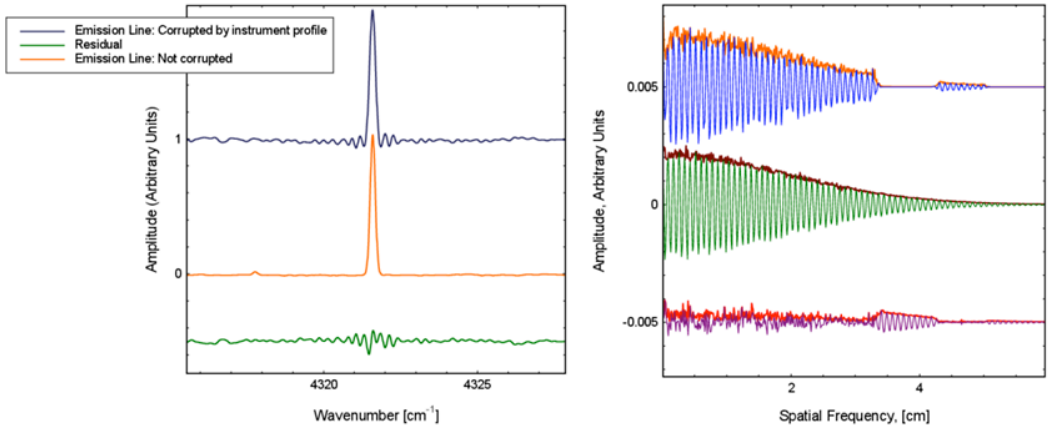

Figure 10. The left panels show lineshape functions that are the Fourier transforms of the MTFs shown in the right panels. The upper curves have a gap in the MTF which results in a lineshape with ringing. The middle curves have a continuous MTF. The lower curves are the differences between the lineshapes and MTFs on the left and right, respectively.

Figure 9 above shows that the addition of the eighth etalon does not provide continuous delay coverage. The consequence of having a gap in the MTF is that the lineshape will have ringing. This is illustrated in Figure 10, where the upper right curve shows the MTF with a gap and the lineshape that results is shown on the left. The middle curves show a continuous MTF and the resulting line with little ringing, and the lower curves show the difference between the MTF curves and the lineshape curves on the right and left, respectively. This picture illustrates the procedure for modeling the missing information in the MTF. If the lines are assumed to be Gaussian, then the difference between what is measured and the model shows the undesired ringing. If the Fourier transform of the lineshape ringing is now subtracted from the MTF of the measurements, a new MTF is formed which has information in the gap.

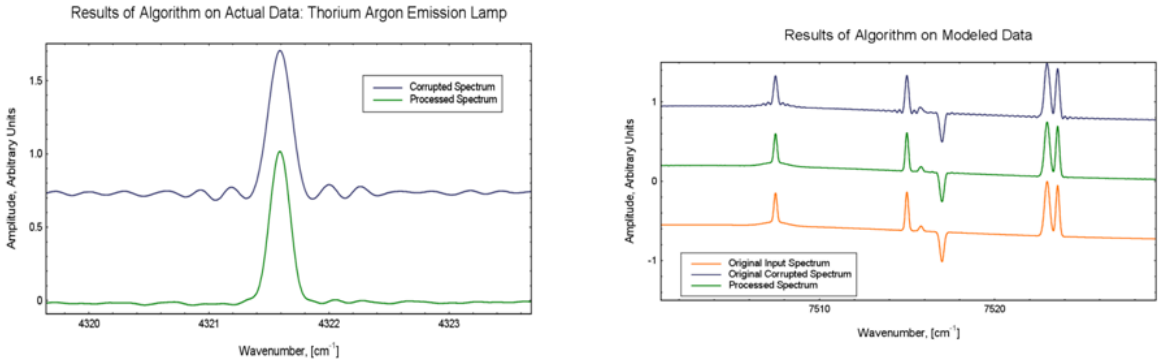

Figure 11. The left panel shows a Th-Ar emission line where the upper curve has a gap in the MTF and the lower curve is the FFT of the MTF which has been filled-in using a Gaussian model for the line. The right panel shows the results of this procedure on simulated data where the upper curve has ringing, the lower curve is the Gaussain line model used to fill-in the MTF, and the middle curve is the spectrum with ringing greatly reduced.

An algorithm has been developed to model emission lines with Gaussians, and subtract the model from the measurements. The Fourier transform of (model-meas) is then subtracted from the Fourier transform of the data (the MTF), but only in the region of the gap. This process is performed iteratively, and only in the gap region so as not to affect the data. In the left panel of Figure 11, a Th-Ar emission line is shown before and after filling in the MTF. The right panel illustrates the removal of ringing in simulated data.

This MTF filling process reduces ringing in high signal-to–noise spectra, but it does not perform quite as well with real data. In Figure 12, the bottom red curve shows the "native" grating spectrum, the top black curve shows the reconstructed spectrum using all eight etalons, and the middle blue curve shows the result of iteratively filling in the MTF gap. In this case ringing in the spectrum is reduced, but not eliminated. This work is still in progress.

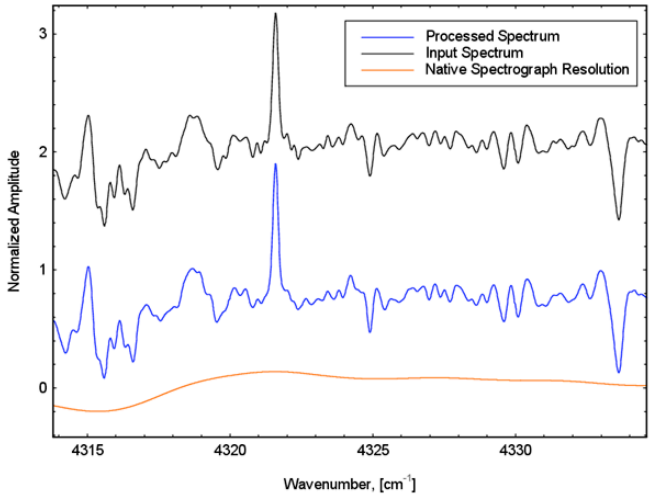

Figure 12. Illustration of filling in the MTF gap using real data. The upper curve is Th-Ar+telluric spectrum obtained from data with a gap in the MTF. The middle curve is the spectrum after filling in the MTF gap using the assumptions that the lines are Gaussian. The bottom curve shows the "native" low resolution grating spectrum.

6. SUMMARY

The EDI technique is being further developed. EDI spectra have been reconstructed with a resolution of 10 times that of the native spectrograph. The accuracy of the reconstructed spectrum is important for spectroscopic measurements requiring good lineshape and continuum information such as measurements of elemental or molecular abundances. Likewise a systematically distorted lineshape could perturb radial velocity measurements. Numerical simulation shows that errors in determining line center frequencies and line widths scale proportionally to errors in the determination of the optical path delay. Some progress has been made in the formulation of algorithms to extrapolate data to portions of the optical delay that may have not been sampled in the MTF.

The strengths of the EDI technique are that a spectrum, or radial velocity, can be measured with an effective resolution much higher than the "native" grating spectrograph. Furthermore, the resolution does not depend on the slit width so the throughput of the grating spectrograph is not limited by this component. For astronomical applications, where facility spectrographs are generally large and expensive, EDI is an attractive technique for extending the spectral resolution of existing instruments.

ACKNOWLEDGMENTS

This work was supported by the National Science Foundation. Observations were conducted at the Mt. Palomar Observatory and the expertise of the support staff is much appreciated. We also benefited from assistance from P. Muirhead, J. Lloyd, and M. Muterspaugh during the observations and analysis.

REFERENCES

[1] D. Erskine, "Combined dispersive/interference spectroscopy for producing a vector spectrum," US Patent 6,351,307, Issued Feb. 26, 2002.

[2] D. Erskine, J. Edelstein, M. Feuerstein, and B. Welsh, "High resolution broadband spectroscopy using an externally dispersed interferometer," ApJ 592, pp. L103–L106, 2003.

[3] D.J. Erskine and J. Edelstein, "Interferometric resolution boosting for spectrographs," in Ground-based Instrumentation for Astronomy, A. Moorwood and M. Iye, eds., Proc. SPIE 5492, pp. 190–199, 2004.

[4] D.J. Erskine, J. Edelstein, P. Muirhead, M. Muterspaugh, K. Covey, D. Mondo, A. Vanderburg, P. Andelson, D. Kimber, M. Sirk, and J. Lloyd, "Ten-fold spectral resolution boosting using TEDI at the Mt. Palomar NIR Triplespec spectrograph," in UV/Optical/IR Space Telescopes and Instruments, L. Tsakalakos, ed., Proc SPIE 8146, pg. 81460M, 2011.

[5] D. Erskine, "An externally dispersed interferometer prototype for sensitive radial velocimetry: theory and demonstration on sunlight," PASP 115, pp. 255–269, 2003.

[6] J. Ge, D. Erskine, and M. Rushford, "An externally dispersed interferometer for sensitive Doppler extra-solar planet searches," PASP 114, pp. 1016–1028, 2002

[7] J. Ge, J. van Eyken, S. Mahadevan, C. DeWitt, S. R. Kane, R. Cohen, A. Vanden Heuvel, S. W. Fleming, P. Guo, G. W. Henry, D. P. Schneider, L. W. Ramsey, R. A. Wittenmyer, M. Endl, W. D. Cochran, E. B. Ford, E. L. Martın, G. Israelian, J. Valenti, and D. Montes, "The first extrasolar planet discovered with a new-generation high-throughput Doppler instrument," ApJ 648, pp. 683–695, 2006.

[8] J. Edelstein, M. Muterspaugh, M. Ward, D. Erskine, M. Feuerstein, M. Marckwordt, E. Wishnow J. Lloyd, T. Herter, P. Muirhead, G. Gull, C. Henderson, S. Parshley, "TEDI: the TripleSpec Exoplanet Discovery Instrument," in Techniques and Instrumentation for Detection of Exoplanets III, D. Coulter, ed., Proc SPIE 6693, pg. 66930W, 2007.

[9] P. S. Muirhead, J. Edelstein, D. J. Erskine, J. T. Wright, M. W. Muterspaugh, K. R. Covey, E. H. Wishnow, K. Hamren, P. Andelson, D. Kimber, T. Mercer, S. P. Halverson, A. Vanderburg, D. Mondo, A. Czeszumska, and J. P. Lloyd, "Precise stellar radial velocities of an M dwarf with a Michelson interferometer and a medium-resolution near-infrared spectrograph," PASP 123(904), pp. 709–724, 2011.

[10] H. G. Roe, Titan's atmosphere at high-resolution. PhD thesis, Univ. California, Berkeley, 2002.